Biochimica et Biophysica Acta 1837 (2014) 131–138

Contents lists available at ScienceDirect

Biochimica et Biophysica Acta

journal homepage: www.elsevier.com/locate/bbabio

Molecular dynamics study of the proposed proton transport pathways in [FeFe]-hydrogenase

Bojana Ginovska-Pangovska, Ming-Hsun Ho, John C. Linehan, Yuhui Cheng, Michel Dupuis, Simone Raugei *, Wendy J. Shaw **

Pacific Northwest National Laboratory, Richland, WA 99352, USA

ARTICLE INFO

Article history:
Received 14 June 2013
Received in revised form 12 August 2013
Accepted 19 August 2013
Available online 24 August 2013

Keywords:
[FeFe]-hydrogenase
Hydrogen bonding
Molecular dynamics
Proton transport
Mutations

ABSTRACT

Possible proton transport pathways in *Clostridium pasteurianum* (CpI) [FeFe]-hydrogenase were investigated with molecular dynamics simulations. This study was undertaken to evaluate the functional pathway and provide insight into the hydrogen bonding features defining an active proton transport pathway. Three pathways were evaluated, two of which consist of water wires and one of predominantly amino acid residues. Our simulations suggest that protons are not transported through water wires. Instead, the five-residue motif (Glu282, Ser319, Glu279, H_2O, Cys299) was found to be the likely pathway, consistent with previously made experimental observations. The pathway was found to have a persistent hydrogen bonded core (residues Cys299 to Ser319), with less persistent hydrogen bonds at the ends of the pathway for both H_2 release and H_2 uptake. Single site mutations of the four residues have been shown experimentally to deactivate the enzyme. The theoretical evaluation of these mutations demonstrates redistribution of the hydrogen bonds in the pathway, resulting in enzyme deactivation. Finally, coupling between the protein dynamics near the proton transport pathway and the redox partner binding regions was also found as a function of H_2 uptake and H_2 release states, which may be indicative of a correlation between proton and electron movement within the enzyme.

1. Introduction

Proton transport pathways play a dominant role in many metalloproteins and serve to deliver protons in a time-controlled fashion between the exterior of the enzyme and the buried active site [1–3]. Despite their broad relevance, the fundamental processes controlling and directing proton transport pathways in biological systems have yet to be fully understood. Indeed, many non-biological systems, for example proton-exchange membranes in fuel cells and electrocatalysts for multi-proton and multi-electron reactions, could also benefit from a fundamental understanding of how to move protons efficiently between distant locations [4].

Hydrogenases are a class of metalloproteins that use a proton transport pathway to assist in the interconversion of hydrogen and protons rapidly and efficiently [Eq. (1)] [1,5,6].

$$H_2 \leftrightarrow 2H^+ + 2e^- \quad (1)$$

Within the H_2 release and uptake hydrogenases there are two general classes: the [NiFe]-hydrogenases, which contain a bimetallic active site composed of Ni and Fe, and the [FeFe]-hydrogenases, which have a bimetallic active site containing two Fe atoms. The efficiency of [FeFe]-hydrogenases as catalysts for H_2 release and their ability to operate bidirectionally has made them a focus of many experimental and theoretical studies in an attempt to extract design principles that can guide the synthesis of efficient molecular catalysts for energy applications.

Clostridium pasteurianum (CpI) [FeFe]-hydrogenase is shown in Fig. 1. The active site of [FeFe]-hydrogenases, the so-called H-cluster, contains a [2Fe]-subcluster, covalently linked to a Fe_4S_4 cubane via a cysteine residue, as shown in Fig. 1 [7–10]. The [2Fe]-subcluster has CO and CN^- ligands on each of the irons, as well as a bridging carbonyl CO group and a bridging di-thiomethylamine (DTMA) group. Protons and electrons are brought to the active site through transport systems. Electron transport is proposed to occur through a series of cubanes (FeS clusters, shown as green and yellow spheres), which originate at redox partner binding sites (Fig. 1, left). Proposed proton transport pathways consist of either primarily water or primarily amino acid residues [11–16], both of which are observed with other metalloproteins [3,12,13,17–20].

The majority of the computational research on [FeFe]-hydrogenase has been focused either on the active site of the enzymes or on characterizing the FeS cubanes that are part of the electron pathway from the

Abbreviations: (CpI), *Clostridium pasteurianum*; (DdH), *Desulfovibrio desulfuricans*; (ESP), Electrostatic potential

* Correspondence to: S. Raugei, P.O Box 999, MS K1-83, Richland, WA 99352, USA. Tel.: +1 509 372 6902.
** Correspondence to: W.J. Shaw, P.O Box 999, MS K2-57, Richland, WA 99352, USA. Tel.: +1 509 375 5922.
E-mail addresses: simone.raugei@pnnl.gov (S. Raugei), Wendy.shaw@pnnl.gov (W.J. Shaw).

0005-2728/$ – see front matter © 2013 Elsevier B.V. All rights reserved.
http://dx.doi.org/10.1016/j.bbabio.2013.08.004

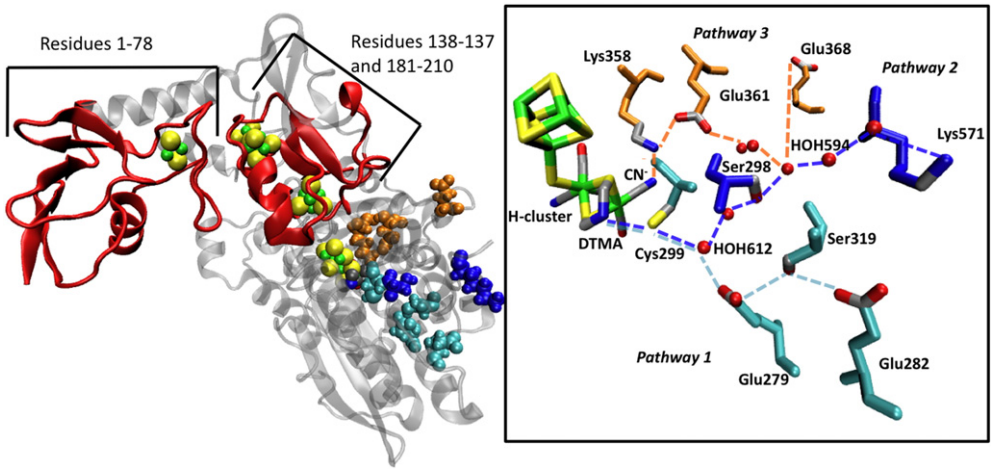

Fig. 1. Left: CpI [FeFe]-hydrogenase with the proposed electron transport (yellow and green spheres) and proton transport (orange, blue or cyan spheres) pathways indicated, along with the redox partner binding regions (red ribbons and brackets). The FeS clusters involved in electron transport are indicated as green and yellow spheres. Right: the three proposed proton transfer pathways are shown in expanded view. Backbone residues in **Pathway 1** are cyan, in **Pathway 2** are blue and in **Pathway 3** are orange. The same colored dashed lines show the proposed proton pathway (double lines are used to show that some residues and water molecules appear in two of the pathways). The color scheme is as follows: green = iron, yellow = sulfur, blue = nitrogen, gray = carbon, and red = oxygen.

surface to the active site, as discussed in recent reviews [1,6]. A less rigorously studied aspect of the catalysis in hydrogenase enzymes has been the mechanism of proton delivery to the active site. There have been several experimental and computational studies of pathways in both [NiFe]-hydrogenase [12–14] and [FeFe]-hydrogenase [11–16], but the mechanism of proton transport is still poorly understood. Studies on [FeFe]-hydrogenases reported so far have focused on the independent investigation of proton and electron pathways. However, the catalytic activity of the enzyme is dependent on the fast and time-controlled delivery of both protons and electrons to the active site. This is often observed to be correlated in other enzymes through a signaling event initiated by long-range structural changes (allosteric interactions). This aspect of the function of hydrogenases is yet to be explored.

In [FeFe]-hydrogenases, three putative proton transport pathways have been proposed (Fig. 1). Each of the three proposed transport pathways terminates at the DTMA or the CN^- ligand of the Fe closest to the proton channel. A proton transport pathway was proposed from the crystallographic structure of CpI that terminates at DTMA and consists of cysteine (C299, numbered according to the Protein Data Bank, PDB ID: 3C8Y [10]), a water molecule (H_2O-612), and two glutamic acids (Glu279 and Glu282) bridged by a serine (Ser319) (**Pathway 1** in Fig. 1, connected with cyan dashed lines) [8]. Biochemical studies on single-site mutations on each of the residues in **Pathway 1** show an almost complete loss of activity in every case, for both H_2 release (>95%) and uptake (>85%) [11,15], demonstrating that the primary structure of that pathway is critical to proton delivery. These investigations provide evidence that **Pathway 1** may be the catalytically active proton transport pathway for [FeFe]-hydrogenase, but they do not eliminate the possibility that alterations in the primary structure in **Pathway 1** may result in structural alterations in other regions of the protein influencing a different proton transport pathway allosterically.

A second proton pathway (**Pathway 2**) was proposed by Hong et al. to contain three crystallographic water molecules (H_2O-594, H_2O-675 and H_2O-668 in CpI), between Ser298 and the surface residue, Lys571 [15]. This transport pathway also shares H_2O-612 and Cys299 with **Pathway 1**, and connects to **Pathway 1** via one more water molecule (H_2O-605). The groups involved in proton transfer in **Pathway 2** are connected by the blue dashed lines in Fig. 1. Protons for both **Pathway 1** and **Pathway 2** are delivered to the DTMA bridge on the active site.

A third proton pathway (**Pathway 3**) has been proposed based on the crystal structure from *Desulfovibrio desulfuricans* (DdH) [FeFe]-hydrogenase, [7] involving the CN^- ligand, residues Lys237, Ser202, Glu240 and three water molecules. A surface residue, Glu245, has also been suggested as a part of this pathway, although it is not strictly conserved among different [FeFe]-hydrogenases. In the CpI hydrogenase, the proton pathway includes Lys358, Ser323 (not shown for clarity in Fig. 1), Glu361, a sequence of water molecules and Glu368 (**Pathway 3**, residues connected with orange lines in Fig. 1; the water molecule H_2O-594 is shared by **Pathway 2** and **Pathway 3**).

In this work, we present a structural and dynamic analysis of the proposed proton delivery pathways to provide mechanistic insight into proton transport. A fundamental hypothesis of our approach is that a well-defined hydrogen bonding network, which can be characterized by features such as stable hydrogen bonding between amino acid residues, hydrogen-bonded water wires, and transient hydrogen bonds facilitated by structural fluctuations, is the basis for efficient proton transfer. Molecular dynamics simulations were performed to investigate the hydrogen bond network in each of the three pathways. Mutations in **Pathway 1** mirroring those in the experimental study by Cornish et al. [11] were also considered in the investigation of the hydrogen bond network and structural alterations of each pathway. These include mutations Cys299 to serine (C299S), Cys299 to alanine (C299A), Glu279 to leucine (E279L), Glu279 to aspartic acid (E279D), Ser319 to alanine (S319A), Glu282 to leucine (E282L) and Glu282 to aspartic acid (E282D) mutations. In addition to these three pathways, previously unidentified pathways that might utilize a water-based pathway to access the active site were explored. Our studies suggest that **Pathway 1** is the most likely proton transport pathway and we evaluated this pathway in more detail. As mentioned above, the correlation of proton and electron movement via allosteric interactions has yet to be explored, and our investigations indicate possible correlations between the electron and proton transport pathway's in the enzyme, suggesting an ever more complex mechanism than currently considered.

2. Methods

2.1. Molecular dynamics (MD) simulations

The enzyme was solvated in a box of ~45000 H_2O molecules, with periodic boundary conditions. For all simulations, the system was first minimized for 1000 steps using conjugate gradient, and then was gradually heated by carrying out 100–200 ps-long equilibrations at increasingly higher temperatures from 0 K to 250 K with increments of 50 K. A simulation was then started at $T = 300$ K, generating trajectories

whose length varied from 80 to 100 ns. The first 10 ns of those trajectories were discarded as the equilibration period. The time step used in the simulations was 2 fs. All simulations were run at constant pressure (1 atm), and constant temperature (298 K) [21,22]. The analysis of the convergence of the simulations reported here is discussed in more detail in the Supplementary Information (Figures S1 and S2).

2.2. Force field parameters

The force field parameters for the MD simulations were taken from the CHARMM [23] force field, and the parameters for the H-cluster and the FeS cubanes were taken from Chang et al. [24]. We modeled the H-cluster in the Fe(I)Fe(I) uptake state, with a vacant coordination site at the distal Fe atom. The charges for the Fe atoms of the H-cluster were calculated using the CP2K program [25] and the scheme proposed by Blöchl [26]. For this calculation we used the DFT PBE functional [27,28], TZVP-MOLOPT-GTH (DZVP-MOLOPT-SR-GTH for Fe) basis set [29] and norm-conserving pseudo-potentials for the interaction of the valence and core electrons [30,31]. The rest of the charges were calculated using the RESP approach in the NWChem program [31] at the B3LYP level of theory and 6-31G* basis set for all atoms except Fe, for which we used the VTZ basis set [32]. Because the original force field parameters have been developed for a structure for the H-cluster where the N atom on the DTMA bridge is not protonated, and the distal Fe atom is bound to an H atom, we adjusted the equilibrium parameters of the force field for the H-cluster (bonds, angles and dihedrals) in order to reproduce two distinct QM optimized geometries (B3LYP/6-31G*; VTZ for Fe): one with one proton on the nitrogen atom of the DTMA bridge, and the second structure with two protons on the nitrogen (DTMA[H^+]). The charges are provided in the Supplementary Information (Figure S3). Protonation states of all of the amino acids were based on a standard pH of 7.0. In the proton pathway, the protonation states are explicitly defined in Figs. 4 and S12.

2.3. Hydrogen bond analysis of **Pathway 1**

A hydrogen bond was considered formed ("occupied") if the distance between the hydrogen bond donor atom and the hydrogen bond acceptor atom was less than 3.5 Å, and the angle occupied by the hydrogen bond donor, the H atom and the hydrogen bond acceptor is larger than 120 degrees.

2.4. Water pathway and water density maps

The analysis of the water paths (hydrogen bonded water wires) was performed by searching for the shortest path between two residues by traversing a network of water molecules connected by hydrogen bonds with a cutoff distance between the oxygen atoms of 3.5 Å. The water density maps were generated as Gaussian-type cube files, containing the frequency with which the center of the oxygen atom of a water molecule occupies a volumetric point (of 0.28 $Å^3$) on a three-dimensional grid. The figures shown represent isodensity surfaces for 5% occupancy. The continuous wire near **Pathway 2** is observed for occupancy of up to ~30%.

2.5. Programs used

The CP2K [25] and NWChem programs [31] were used for the quantum mechanical calculations. All classical MD simulations were carried out using the NAMD program [34]. The analysis of the hydrogen bonds was carried out using VMD [33]. Residues root mean square displacement, root mean square fluctuations, and covariance maps were generated using Gromacs tools. The electrostatic potential maps were calculated by solving the Poisson–Boltzmann equation using the APBS program [35]. The pK_a values were calculated with PROPKA 3.1 [36].

3. Results and discussion

3.1. Evaluation of the **Pathways** for their role in proton delivery

Our initial goal was to establish the predominant proton pathway among the three proposed pathways. Reported experimental data show that point mutations in **Pathway 1** result in a severe loss of function, [11] which could be due to a disruption of the hydrogen bonding network in the pathway, but it could also result from allosteric structural influences on other regions of the protein, altering another operative, distant pathway. There are many crystallographic waters in the protein, and our molecular dynamics simulations show a high volume of water within the interior of the protein. To gain a better understanding of the possibility of water pathways in proton delivery, including **Pathways 2** and **3** from Fig. 1, we analyzed the space in the enzyme occupied by water molecules.

During the simulations, the positions of all of the water molecules on the inside of the enzyme were tracked to identify stable water channels connecting the active site to the surface of the enzyme. The resulting water density map is shown in Figure S4, with the majority of the surface waters removed for clarity of presentation. The water density near the three proposed pathways is shown in Fig. 2. A water-rich pocket is identified involving the water molecules from the -two water pathways described above (Fig. 2, red), allowing water to access residues Ser298 and Cys299, providing a direct pathway from the surface to deliver protons to the DTMA. The full water density map (Figure S4) shows that the cavity on the opposite side of the H-cluster is hydrophobic, in agreement with the suggestion that water only approaches the active site from the above mentioned water pocket. Although in the crystal structure a water molecule was found to bind to the distal iron atom (not coordinating with the FeS cluster) off the 2Fe-subcluster, this water quickly leaves in the course of the simulation. Multiple pathways allow water to penetrate from the enzyme surface to this pocket and exchange with the water therein, but among all of the possible pathways, **Pathway 2** is the shortest route from the surface to the active site, indicating that no additional pathways besides those shown in Fig. 1 need to be considered. It can also be observed in Fig. 2 that **Pathway 1** does not have a water wire running adjacent to it, confirming that if **Pathway 1** is the active proton transport pathway, it is the amino acid residues themselves participating in the proton transport, and the mechanism does not involve a proximally placed water wire as has been proposed for other systems [37,20].

Further establishing the relevant proton transport pathway(s) includes studying the structural stability of the residues and the stability of the hydrogen bonding network for each of the pathways and how these change as a function of mutation. Because the mutations introduced in **Pathway 1** experimentally deactivate the enzyme, they are expected to introduce structural differences and/or differences in the hydrogen bonding network in the functional proton transport pathway. Both **Pathway 2** and **Pathway 3** contain water wires, assumed to connect residues from the surface of the enzyme (Lys571 or Glu368, respectively) to residues near the active site (Ser298 or Glu361, respectively). The stability of the water wire hydrogen bonding network was evaluated for these pathways by assessing the length and stability of the network that could potentially be involved in proton delivery, and how mutations in **Pathway 1** affect the stability of those networks. The structural stability of the residues involved in those channels was also investigated.

To evaluate whether mutations of residues in **Pathway 1** (C299S, C299A, E279L, E279D, S319A, E282L, E282D) have an effect on the water path in **Pathway 2**, the distance between residues Ser298 and Lys571, both of which belong to **Pathway 2**, was measured and found to be independent of mutation (12.8 ± 1.5 Å), reflecting insensitivity of the water path in **Pathway 2** to the mutations in **Pathway 1**. Additionally, no significant structural distortions were observed in the region of either Ser298 or Lys571, or the residues surrounding the water

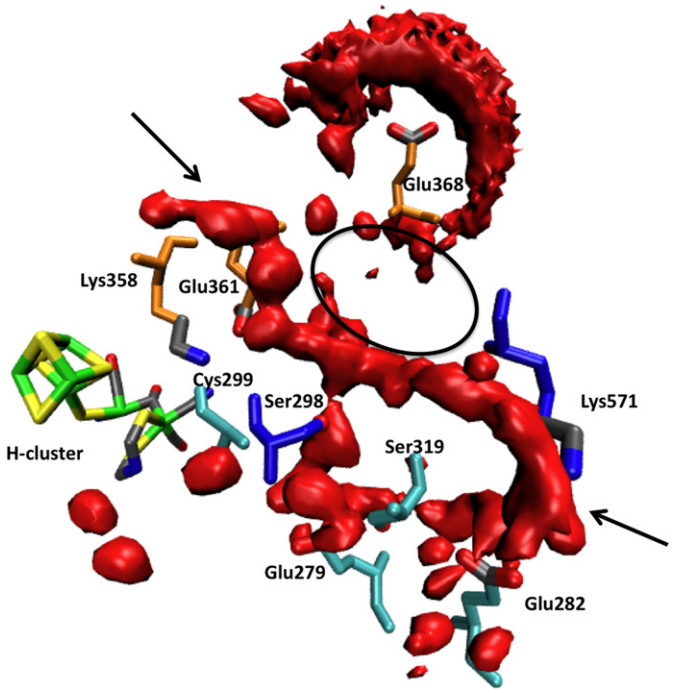

Fig. 2. Water density map of the [FeFe]-hydrogenase showing all of the water pathways (red) from the protein surface to the active site. The pathways converge to a water pocket (indicated with black arrows), part of which corresponds to **Pathway 2** (residues in blue). **Pathway 3** (orange) has a hydrophobic pocket (shown with a black oval) disrupting the flow of protons from the surface to the active site. **Pathway 1** (cyan) has water present but not enough to allow protons to transfer without the assistance of residues. None of the other waters in the scaffold form a continuous pathway from the surface of the protein to the active site, suggesting that no additional pathways need to be considered (Figures 2 and S4).

pocket, further establishing the structural insensitivity of **Pathway 2** to mutations in **Pathway 1**. The hydrogen bonding network was also analyzed between Ser298 and Lys571 by identifying the shortest path of hydrogen bonded water molecules. Bar graphs showing the average length of the water paths are available in the Supplementary Material (Figure S5). When Glu279 is protonated (expected in the resting state of the enzyme as described in Section 3.2), the mutated enzymes have an average water path length ranging from 5.6 to 8.6 water molecules, with standard deviations of 1.7 to 2.3 waters depending on mutation. No clear trend was observed in the length of the water path as a result of the mutations of the residues in **Pathway 1**, i.e. some of the mutations resulted in a slightly longer average water path length, while some were slightly shorter. However, differences were always smaller than the standard deviation from the average and therefore not statistically meaningful. Collectively, these observations suggest that **Pathway 2** is not a key pathway for proton delivery, since the mutations in **Pathway 1** that are known to hinder the catalytic activity of the enzyme, have no measurable effect on the structure or hydrogen bonding pathway between the key residues in **Pathway 2.** This is consistent with the experimental observation that mutation of Ser298 does not alter activity [11].

A similar analysis was performed for the water wires between residues Glu361 and Glu368 in **Pathway 3**. In the DdH structure, the side chain of the corresponding Glu245 is oriented towards the interior of the protein and is hydrogen bonded to the crystallographic water near Glu240 (residue Glu361 in CpI, Fig. 1) [7]. In CpI, the side chain for Glu368 is rotated and points away from the interior of the protein, disrupting the hydrogen bonding of the water wire to the active site [8]. Consistent with a surface orientated sidechain for Glu368 is that all water paths were longer than 10 water molecules for this pathway, and in each case included bulk water on the exterior of the protein to complete the pathway. Further, analysis of the water within the enzyme shows that the space between Glu361 and Glu368 is a hydrophobic domain bordered by residues Met367, Ala362 and Gln326. This ~6 Å diameter domain excludes water, eliminating a direct water wire between the two residues (Fig. 2). Additionally, mutations did not influence the distance between Glu361 and Glu368 (15.5 ± 1.1 Å), showing that mutations in **Pathway 1** do not affect the structural stability in **Pathway 3**. Therefore, all of the simulations are consistent with this pathway not being important for proton transport. The study by Happe et al. on residue Lys358, which was proposed as part of **Pathway 3,** found that mutating this residue to an asparagine inactivated the enzyme for both H_2 uptake and release, due to the structural alteration in the active site [38]. The modeling results shown here support those authors suggestion that Lys358 plays a role in maintaining structural stability at the active site, rather than delivering protons to the active site.

To further evaluate the most likely proton transport pathway, the electrostatic potential (ESP) at the surface of the enzyme for the crystal structure of the CpI enzyme was determined (Fig. 3). In the native enzyme, there is a well-defined region of negative potential around the surface-exposed Glu282 residue at the entrance to **Pathway 1**, ideal for attracting protons into the pathway. Nearby are more positive electrostatic regions, part of which corresponds to residue Arg286. The presence and role of this residue will be discussed in more detail in Section 3.2. Importantly, the entrance of **Pathway 2** has a positive electrostatic potential (green circle in Fig. 3), as expected from the presence of the positively charged Lys571, making this entrance unfavorable for proton entry.

Collectively, the structural, hydrogen bonding and electrostatic analyses are all highly suggestive that **Pathways 2** and **3,** the water-containing pathways, are not the predominant proton transport pathways. It is intriguing that the water wires are not the likely active proton transport pathway in this [FeFe]-hydrogenase, since a water wire is a proton transfer mechanism used by many other enzymes and has the advantages of not being affected by mutations and of requiring low reorganization energies [3]. In addition, computational studies of proton transfer in short water-wires (2–4 water molecules) have shown that proton transfer can occur very fast (on the femtosecond scale) [39,40]. On the other hand, it has been observed that forming the Eigen cation ($H_9O_4^+$) is an energetic trap [3,40,41]. The Eigen cation would be favored by large water pockets such as the one observed here, [39] whereas the Zundel cation ($H_5O_2^+$) is favored in discrete water wires, [40] and may explain why water in this case is not a functional proton transport mechanism. While it is not clear why a predominately residue-based pathway is preferred over a water-based pathway in [FeFe]-hydrogenase, it is interesting

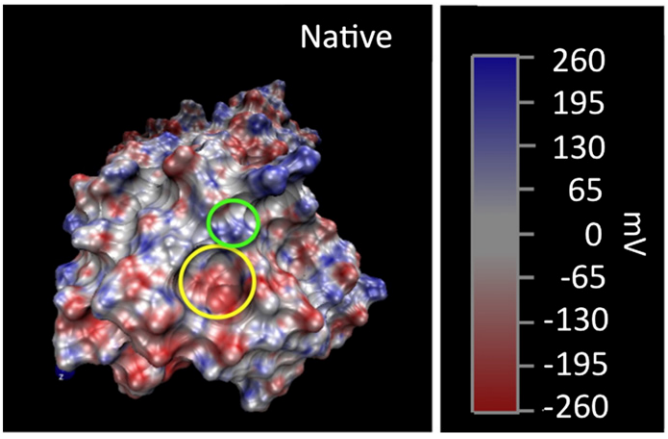

Fig. 3. Electrostatic potential maps of the native [FeFe]-hydrogenase enzyme. The potential is projected on the van der Waals surface of the enzyme. The green circle marks the location of Lys571, the entrance to **Pathway 2** and the yellow circle indicates Glu282, the entrance to **Pathway 1.** Regions of positive electrostatic potential are colored in blue, and regions of negative electrostatic potential are colored in red. The negative electrostatic potential at the mouth of **Pathway 1** emphasizes the favorable electrostatic environment for proton uptake.

to note that the proposed pathway for a [NiFe]-hydrogenase is a residue based pathway [12,13].

3.2. **Pathway 1**: *characterization of the hydrogen bonding network*

The insensitivity of the structure and the hydrogen bonding network in **Pathways 2** and **3** to mutations in **Pathway 1** strongly suggest that **Pathway 1** is the best candidate for proton delivery. To understand the features that might make it a good proton transfer pathway and to provide insight into why mutation causes catalytic failure, we characterized the hydrogen bonding network, which has been shown to be important for efficient proton transfer [3,37,42]. **Pathway 1** was modeled in the presence of protons (Fig. 4), and the choice of protonation states was based on two factors, the pK_a of the residues in the pathway and the likely resting state of the protons on those residues. Based on the predicted pK_a value for Glu279 (8.5), this residue is expected to be protonated at all times and is left protonated in our simulations (the pK_a of Glu282 is predicted to be 5.2 and is not expected to be protonated in the resting state). The protonatable residues are Glu282, Glu279 and DTMA, while proton movement between these residues is mediated by Ser319, Cys299 and the H_2O molecule, where the proton is not likely to reside. Based on these predictions, two doubly protonated states are considered, one for H_2 release with Glu282 and Glu279 protonated (Fig. 4, left) and one for H_2 uptake with Glu279 and the DTMA protonated (Fig. 4, right). The hydrogen bonding network observed for each protonation state is consistent with the proposed proton delivery direction, as shown with the dotted lines in Fig. 4. These protonation schemes imply a fully concerted Grotthuss-like proton transfer, as shown by the arrows in Fig. 4. For completeness, we also considered single protonation states, where the proton may reside on Glu282 or DTMA, as well as different initial protonation sites, where DTMA and Glu282 are protonated, the results of which are provided in the supplementary information (Figures S12 to S24).

We characterized the hydrogen bond network using the occupancy of four hydrogen bonds in **Pathway 1:** a) DTMA to Cys299; b) Cys299–HOH–Glu279; c) Glu279 to Ser319 and d) Ser319 to Glu282. Occupancy is defined as the percentage of structures that show a hydrogen bond once thermal equilibration has been reached (after 10 ns), based on 75–100 ns of data. The occupancy can have values from 0% to 200%, with values greater that 100% possible only for the Glu residues, which offer two hydrogen bonding sites. The hydrogen bond occupancies for H_2 release and for H_2 uptake are shown in Fig. 4.

As seen in Fig. 4, hydrogen bonding is very low between Ser319–Glu282 in both cases (<10%), but is high between Glu279–Ser319 and Cys299–HOH–Glu279, with an occupancy ranging from 40% to 50% for both hydrogen bonds for both H_2 release and uptake. Hydrogen bonding between DTMA–Cys299 is much lower (<5%) for the H_2 uptake direction compared to the H_2 release direction, which has an occupancy of ~70%, and may point to the importance of fluxional hydrogen bonds being related to the reversibility of the proton channel. These observations suggest that overall, a continuous hydrogen bonding pathway capable of a Grotthuss-like transport to and from the active site is possible, with hydrogen bonding at the ends of the pathway being highly fluxional and in the central portion of the pathway being more persistent.

Investigation of the low occupancy of the hydrogen bonds between Glu282 and Ser319 at the entrance to the proton channel revealed

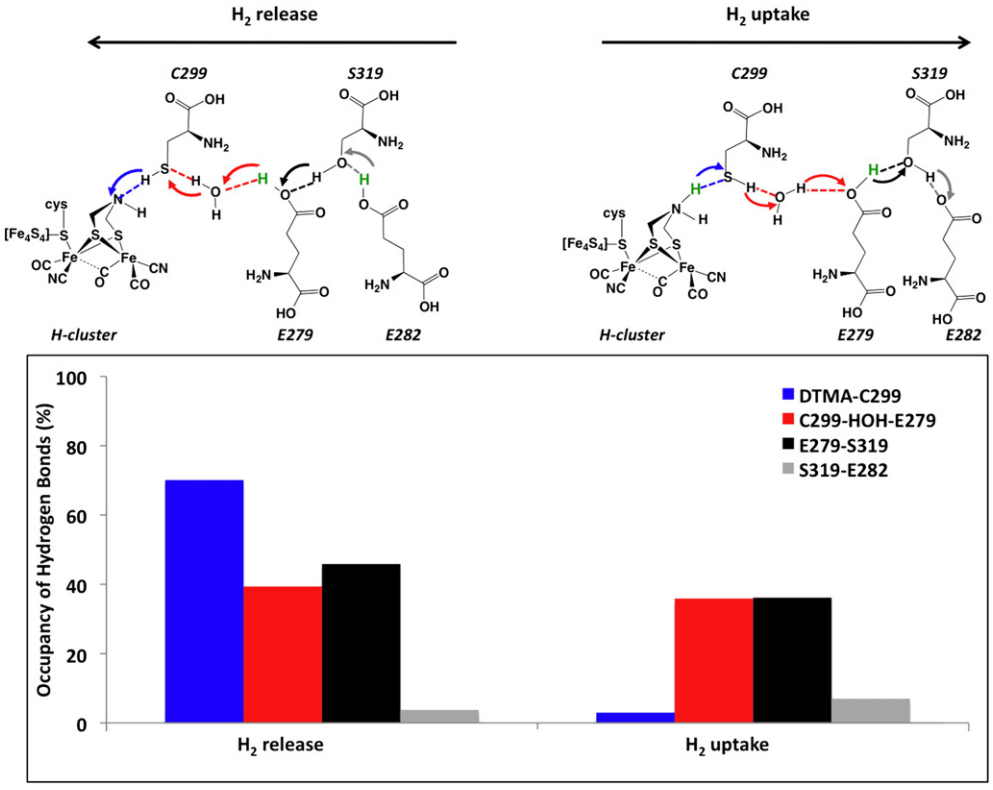

Fig. 4. Top: **Pathway 1** was protonated in two different ways to investigate the hydrogen bonding network. In the H_2 release system (left), the protons start on Glu282 and Glu279 (shown in green) and transfer in one concerted step (shown with arrows, using the same color coding as the hydrogen bonds on the bottom panel) to the active site. In the H_2 uptake system (right), the excess protons start on Glu279 and DTMA (shown in green) and transfer in one concerted step to the surface of the enzyme. **Bottom**: The occupancy of the hydrogen bonds between the residues in **Pathway 1** for H_2 release (left) and uptake (right). Each hydrogen bond in the pathway is shown in a different color. The columns for Cys299–HOH–Glu279 show the simultaneous occupancy of hydrogen bonding between Glu279–HOH and HOH–Cys299. The differences in the hydrogen bonding patterns for H_2 uptake and release suggest that the fluctuations of the DTMA–Cys299 and the Ser319–Glu282 hydrogen bonds depend on the location of the proton, whereas the Cys299–HOH–Glu279 and Glu279–Ser319 hydrogen bonds are less sensitive. The hydrogen bonds shown would be present during proton transfer, but may only be transiently observed in the resting state.

that it is due to the presence of a nearby, positively charged arginine residue (Arg286) which forms a strong salt bridge (with the occupancy of the hydrogen bond always >100%) with the non-protonated Glu282, preventing the interaction with the rest of the proton channel. Protonation of Glu282 almost eliminates the interaction with Arg286, reducing the occupancy of this hydrogen bond to 9%. Even in this case, Glu282 infrequently hydrogen bonds with Ser319, but largely hydrogen bonds with the solvent and to some extent, with another serine residue (Ser320), with the hydrogen bond occupancy of 4% for H_2 release and 60% for H_2 uptake. Evaluation of the Arg286 to leucine (R286L) mutation with molecular dynamics also eliminates the salt bridge with Glu282 and makes the electrostatic potential more negative (Figure S6), features that would be expected to enhance proton delivery to the active site. These observations suggest that both Arg286 and Ser320 may be relevant to proton delivery and catalysis; further experimental studies are needed to assess their importance.

Our simulations suggest that high hydrogen bond occupancy is not always required for facile proton transfer. This is particularly evident for residue Glu282, where a limited occupancy is typically observed. Experimentally, we know this residue is essential and therefore conclude that a transient interaction is achieved with enough frequency ($\sim 10^4$ s^{-1}, based on the reported rate of 9000 s^{-1} for H_2 release [43]) to achieve adequate proton transport. Fast proton transfer has been observed in a molecular catalyst where protons move intramolecularly at 10^5–10^6 s^{-1} even with a significant structural rearrangement, when the hydrogen bond donors and acceptors can achieve proper positioning [44]. Although the timescale of the observed catalytic rates (microseconds) differs from the simulated timescale (nanoseconds), the MD simulations suggest that the hydrogen bonding patterns observed here are relevant to those that would be found on the catalytic timescale. Specifically, the presence of the more persistent hydrogen bonding in the central region and the fluctuations at the ends of the pathways observed at shorter timescale both facilitate proton transport.

3.3. Hydrogen bonding in **Pathway 1** as a function of single-site mutations

To provide insight into why mutations in the pathway result in catalyst deactivation, we have extended our molecular dynamics study to investigate changes in hydrogen bonding as a function of the mutations that have been shown experimentally to result in a nearly complete inactivation of enzymatic activity for H_2 release, and in a large inactivation (>85%) for H_2 uptake [11]. Our simulations show that catalytic inactivation can be explained by a disruption in the hydrogen bonding network. The mutations alter hydrogen bonding in the proton transport pathway in one of two ways. The most intuitive deactivation is achieved by introducing a mutation with no hydrogen bond capabilities (for example by mutating the serine residue to alanine), thereby disrupting the hydrogen bonding network and the ability to transfer protons. Data of the resulting occupancy of the hydrogen bonds are provided in the supplementary information (Figure S7).

The more interesting mutations are those in which the mutation allows hydrogen bonding (for example when cysteine is mutated to serine), but still results in catalyst deactivation. The results for these mutations (C299S, E279D and E282D) are shown in Fig. 5 for the two protonation states. The level of interruption is highly dependent on both the protonation state and the nature of the mutation. No significant structural change is observed for the backbone residues in the proton pathway under any condition, removing this as a cause for inactivity.

For both H_2 release and H_2 uptake, the hydrogen bond between Glu282 and Ser319 is negligible, consistent with observations for the native enzyme. The E282D mutant has the most dramatic effect of the hydrogen bonding network, eliminating all hydrogen bonds except Glu279–Ser319, which is more than doubled in occupancy over the native hydrogen bond for both H_2 release and uptake. The C299S mutant also significantly affected the hydrogen bonding patterns for both H_2 release and uptake. For H_2 uptake, the hydrogen bonding pattern is similar to that observed for E282D, where the Glu279–Ser319 hydrogen bond increases to 90% with very little occupancy in the other hydrogen bonds. For H_2 release, the C299S mutant results in an increase in both DTMA–Cys299 and Glu279–Ser319 and a reduction in Cys299–HOH–Glu279 and Ser319–Glu282. The E279D mutant for H_2 release results in an almost total loss of the Cys299–HOH–Asp279 hydrogen bond and a 50% reduction of Asp279–Ser319 hydrogen bond. The effect of E279D on H_2 uptake was less dramatic, where the Cys299–HOH–Glu279 reduced by 50% but the other hydrogen bonds were not affected significantly. Because no changes in the backbone structure are observed, the observed differences in the hydrogen bonding may be due to the shorter side chain length in the case of mutating glutamic acid to aspartic acid resulting in distances that do not accommodate the O—H…O hydrogen bond, or changes in the local electrostatics. For the cysteine to serine mutation, the introduction of a residue with a non-optimized (stronger) pK_a, which alters the desired hydrogen bonding network, may be the cause for changes in the hydrogen bonding. While there is no consistent change in the hydrogen bonding network as a function of mutation, the data in Fig. 5, coupled with the experimental observations [11], suggest that even minor disruptions in the hydrogen bonding network (i.e., E279D, H_2 uptake) can result in significant losses (>85%) in catalytic activity.

3.4. Coupling of protonation in the proton channel with the binding of the redox partner?

In many metalloenzymes, proton movement is often hypothesized to be coupled with electron transport through allosteric mechanisms. The evaluation of structural changes throughout the protein was

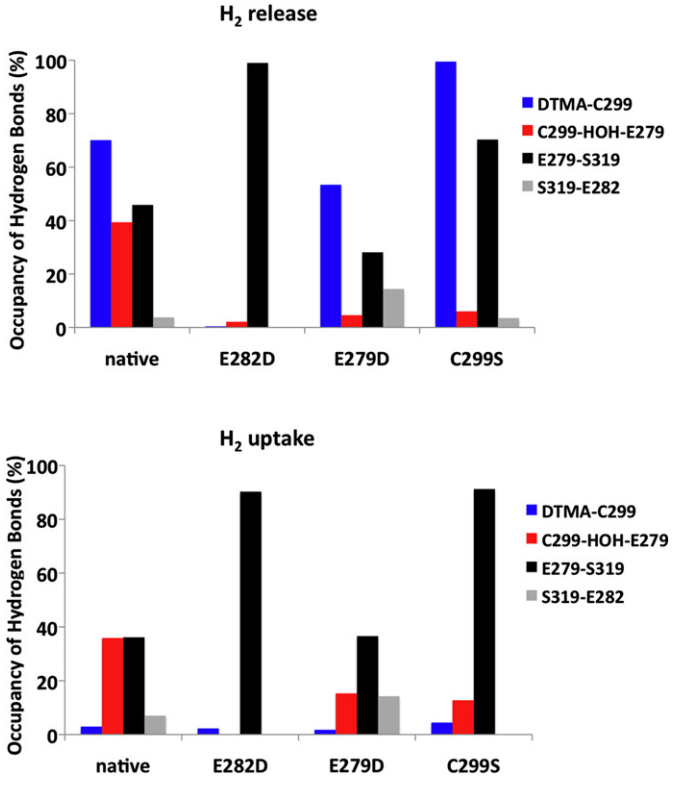

Fig. 5. Hydrogen bonding occupancies (*Y*-axis) as a function of mutation (*X*-axis) for H_2 release (top) and H_2 uptake (bottom). Each hydrogen bond in the pathway is shown as a different color, as indicated in the legend and analogous to Fig. 4. The E282D mutant had the largest impact on the hydrogen bonding network for both H_2 release and H_2 uptake, disrupting all hydrogen bonds with the exception of the stable Glu279–Ser319 hydrogen bond.

undertaken to provide insight into a correlation between proton and electron transport. Large amplitude displacements in the enzyme as a function of the H_2 uptake and release states were observed by calculating the root mean square fluctuations, the results of which are shown in Fig. 6. This analysis shows that the largest fluctuations in the enzyme resulting from the two different protonation states take place either at the mouth of the proton channel (H_2 uptake), or far from the proton channel, in the regions that are known to be redox partner binding sites [45] (H_2 uptake and H_2 release). Since the backbone of the residues in the proton transport pathway do not show any significant structural change as a function of protonation state or mutation, these results suggest that the enzyme responds to protonation within the proton transport pathway by undergoing increased fluctuations both near the mouth of the pathway and the electron channel, possibly to signal a binding event from the redox partner. This may be indicative of a coupling mechanism between proton motion within the enzyme and the binding (dissociation) of the redox partner, therefore, suggesting a possible role in controlling electron transfer to the enzyme.

3.5. The effects of mutation on the protein motion

Considering the same mutations that were evaluated for changes in hydrogen bonding, we observed that the backbone dynamics are sensitive to mutation (Figures S8 and S9). For the H_2 release system, the most notable trend is that the backbone motions are maintained or reduced for all mutations, and are never larger than the motions of the native enzyme. The opposite trend is observed for the H_2 uptake system, where mutants have either similar or more intense backbone motions than the native enzyme. The most significant change was found in the S319A mutant, where the flexibility of the residues near both the entrance to **Pathway 1** and the electron channel is increased dramatically (Figure S9). This observation may suggest that mutations not only have the effect of breaking the hydrogen bond network, but may also influence electron transfer between hydrogenase and its redox partner. Further evidence that changes in the proton channel can induce a response in the electron channel is supported by the observed correlation in the motions of the different parts of the enzyme represented by covariance maps (Figures S10 and S11). It is not possible to quantitatively assess the functional relevance of the correlated and anti-correlated motion with the current studies, but this correlation further supports the idea that events in **Pathway 1** modulate redox processes with the enzyme redox partner.

4. Summary

Possible proton transport pathways of CpI [FeFe]-hydrogenase have been studied using molecular dynamics simulations. The results are consistent with a pathway containing predominantly amino acid residues being the dominant proton transfer pathway, rather than a water-based pathway. The residue-based pathway was studied in more detail as a function of protonation state and mutation to provide insight into why mutation causes catalytic failure. A continuous hydrogen bond network was identified throughout this pathway, with a stable central region and more flexible terminal regions. Mutations of the residues in this pathway result in an interruption of the hydrogen-bonding network, consistent with the experimentally observed loss in catalytic activity. A possible role is proposed for two additional residues at the entrance of the proton transfer pathway (Ser320 and Arg286) that could be tested by experimental mutation studies. It was also clear that different proton placement in the pathway results in changing motions in the redox-partner binding region that may indicate coupling between the proton and electron transfer processes in spite of their spatial separation. This work provides the foundation for future work in evaluating the mechanism for proton transfer through this active pathway.

Acknowledgements

The authors would like to thank Eric Hegg and Adam Cornish for useful discussions. This work was funded by the DOE Office of Science Early Career Research Program through the Office of Basic Energy Sciences. Computational resources were provided at W. R. Wiley Environmental Molecular Sciences Laboratory (EMSL), a national scientific user facility sponsored by the Department of Energy's Office of Biological and Environmental Research located at Pacific Northwest National Laboratory, and a portion of the research was performed using PNNL Institutional Computing at Pacific Northwest National Laboratory. Pacific Northwest National Laboratory is operated by Battelle for the U.S. Department of Energy. Supporting materials may be accessed free of charge online at http://pubs.acs.org.

Appendix A. Supplementary data

Supplementary data to this article can be found online at http://dx.doi.org/10.1016/j.bbabio.2013.08.004.

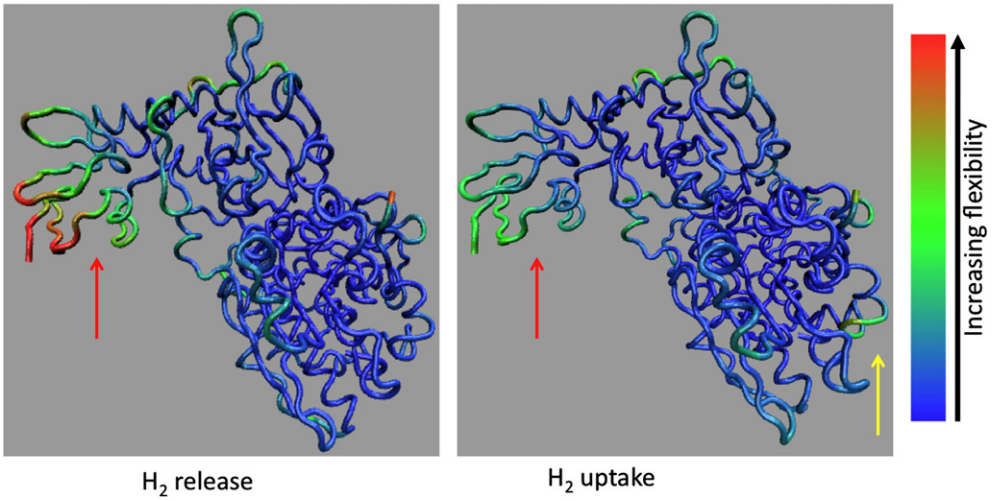

Fig. 6. Regions of high backbone flexibility for the H_2 release and H_2 uptake systems are shown in red and green, where larger amplitude motion is shown as follows: blue < green < red. The yellow arrow shows the entrance to **Pathway 1**. In general, the H_2 release system (left) exhibits more flexibility in the redox partner binding regions (red arrow) than in the uptake system (right), while the uptake system has more flexibility near the mouth of the proton channel (yellow arrow).

References

[1] J.C. Fontecilla-Camps, A. Volbeda, C. Cavazza, Y. Nicolet, Structure/function relationships of [NiFe]- and [FeFe]-hydrogenases, Chem. Rev. 107 (2007) 4273–4303.
[2] A. Guskov, J. Kern, A. Gabdulkhakov, M. Broser, A. Zouni, W. Saenger, Nat. Struct. Mol. Biol. 16 (2009) 334–342.
[3] C.A. Wraight, Chance and design—proton transfer in water, channels and bioenergetic proteins, Biochim. Biophys. Acta 1757 (2006) 886–912.
[4] O. Diat, G. Gebel, Proton channels, Nat. Met. 7 (2008) 13–14.
[5] J.-F. Capon, F. Gloaguen, F.Y. Petillon, P. Schollhammer, J. Talarmin, Electron and proton transfers at diiron dithiolate sites relevant to the catalysis of proton reduction by the [FeFe]-hydrogenases, Coord. Chem. Rev. 253 (2009) 1476–1494.
[6] P.E.M. Siegbahn, J.W. Tye, M.B. Hall, Computational studies of [NiFe] and [FeFe] hydrogenases, Chem. Rev. 107 (2007) 4414–4435.
[7] Y. Nicolet, C. Piras, P. Legrand, C.E. Hatchikian, J.C. Fontecilla-Camps, *Desulfovibrio desulfuricans* iron hydrogenase: the structure shows unusual coordination to an active site Fe binuclear center, Struct. Fold. Des. 7 (1999) 13–23.
[8] J.W. Peters, W.N. Lanzilotta, B.J. Lemon, L.C. Seefeldt, X-ray crystal structure of the Fe-only hydrogenase (Cpl) from *Clostridium pasteurianum* to 1.8 angstrom resolution, Science 282 (1998) 1853–1858.
[9] Y. Nicolet, B.J. Lemon, J.C. Fontecilla-Camps, J.W. Peters, A novel FeS cluster in Fe-only hydrogenases, Trends Biochem. Sci. 25 (2000) 138–143.
[10] A.S. Pandey, T.V. Harris, L.J. Giles, J.W. Peters, R.K. Szilagyi, Dithiomethylether as a ligand in the hydrogenase H-cluster, J. Am. Chem. Soc. 130 (2008) 4533–4540.
[11] A.J. Cornish, K. Gartner, H. Yang, J.W. Peters, E.L. Hegg, Mechanism of proton transfer in [FeFe]-hydrogenase from *Clostridium pasteurianum*, J. Biol. Chem. 286 (2011) 38341–38347.
[12] I.F. Galvan, A. Volbeda, J.C. Fontecilla-Camps, M.J. Field, A QM/MM study of proton transport pathways in a [NiFe]-hydrogenase, Proteins Struct. Funct. Bioinform. 73 (2008) 195–203.
[13] V.H. Teixeira, C.M. Soares, A.M. Baptista, Proton pathways in a [NiFe]-hydrogenase: a theoretical study, Proteins Struct. Funct. Bioinform. 70 (2008) 1010–1022.
[14] I. Sumner, G.A. Voth, Proton transport pathways in [NiFe]-hydrogenase, J. Phys. Chem. B 116 (2012) 2917–2926.
[15] G. Hong, A.J. Cornish, E.L. Hegg, R. Pachter, On understanding proton transfer to the biocatalytic [Fe–Fe]H sub-cluster in [Fe–Fe] H2ases: Qm/MM MD simulations, Biochim. Biophys. Acta 1807 (2011) 510–517.
[16] S. Morra, A. Giraudo, G. Di Nardo, P.W. King, G. Gilardi, F. Valetti, Site saturation mutagenesis demonstrates a central role for cysteine 298 as proton donor to the catalytic site in CaHydA [FeFe]-hydrogenase, PLoS One 7 (2012) e48400.
[17] T. Yamshita, G.A. Voth, Insights into the mechanism of proton transport in cytrochrome c oxidase, J. Am. Chem. Soc. 134 (2011) 1147–1152.
[18] J. Xu, G.A. Voth, Computer simulation of explicit proton translocation in cytochrome c oxidase: the D-pathway, Proc. Natl. Acad. Sci. U. S. A. 102 (2005) 6795–6800.
[19] B. Roux, Computational studies of the gramicidin channel, Acc. Chem. Res. 35 (2002) 366–375.
[20] Y.Y. Sham, I. Muegge, A. Warshel, Simulating proton translocations in proteins: probing proton transfer pathways in the *Rhodobacter sphaeroides* reaction center, Proteins Struct. Funct. Bioinform. 36 (1999) 484–500.
[21] S.E. Feller, Y.H. Zhang, R.W. Pastor, B.R. Brooks, Constant-pressure molecular-dynamics simulation — the Langevin piston method, J. Chem. Phys. 103 (1995) 4613–4621.
[22] G.J. Martyna, D.J. Tobias, M.L. Klein, Constant-pressure molecular-dynamics algorithms, J. Chem. Phys. 101 (1994) 4177–4189.
[23] A.D. MacKerell, D. Bashford, M. Bellott, R.L. Dunbrack, J.D. Evanseck, M.J. Field, S. Fischer, J. Gao, H. Guo, S. Ha, D. Joseph-McCarthy, L. Kuchnir, K. Kuczera, F.T.K. Lau, C. Mattos, S. Michnick, T. Ngo, D.T. Nguyen, B. Prodhom, W.E. Reiher, B. Roux, M. Schlenkrich, J.C. Smith, R. Stote, J. Straub, M. Watanabe, J. Wiorkiewicz-Kuczera, D. Yin, M. Karplus, All-atom empirical potential for molecular modeling and dynamics studies of proteins, J. Phys. Chem. B 102 (1998) 3586–3616.
[24] C.H. Chang, K. Kim, Density functional theory calculation of bonding and charge parameters for molecular dynamics studies on [FeFe] hydrogenases, J. Chem. Theory Comput. 5 (2009) 1137–1145.
[25] J. VandeVondele, M. Krack, F. Mohamed, M. Parrinello, T. Chassaing, J. Hutter, QUICKSTEP: fast and accurate density functional calculations using a mixed Gaussian and plane waves approach, Comput. Phys. Commun. 167 (2005) 103–128.
[26] P.E. Blochl, Electrostatic decoupling of periodic images of plane-wave-expanded densities and derived atomic point charges, J. Chem. Phys. 103 (1995) 7422–7428.
[27] J.P. Perdew, K. Burke, M. Ernzerhof, Generalized gradient approximation made simple, Phys. Rev. Lett. 77 (1996) 3865–3868.
[28] J.P. Perdew, K. Burke, M. Ernzerhof, Generalized gradient approximation made simple (vol 77, pg 3865, 1996), Phys. Rev. Lett. 78 (1997) 1396.
[29] J. VandeVondele, J. Hutter, Gaussian basis sets for accurate calculations on molecular systems in gas and condensed phases, J. Chem. Phys. 127 (2007).
[30] S. Goedecker, M. Teter, J. Hutter, Separable dual-space Gaussian pseudopotentials, Phys. Rev. B 54 (1996) 1703–1710.
[31] M. Valiev, E.J. Bylaska, N. Govind, K. Kowalski, T.P. Straatsma, H.J.J. Van Dam, D. Wang, J. Nieplocha, E. Apra, T.L. Windus, W. de Jong, NWChem: a comprehensive and scalable open-source solution for large scale molecular simulations, Comput. Phys. Commun. 181 (2010) 1477–1489.
[32] A. Schafer, H. Horn, R. Ahlrichs, Fully optimized contracted Gaussian-basis sets for atoms Li to Kr, J. Chem. Phys. 97 (1992) 2571–2577.
[33] W. Humphrey, A. Dalke, K. Schulten, VMD: visual molecular dynamics, J. Mol. Graph. Model. 14 (1996) 33–38.
[34] J.C. Phillips, R. Braun, W. Wang, J. Gumbart, E. Tajkhorshid, E. Villa, C. Chipot, R.D. Skeel, L. Kale, K. Schulten, Scalable molecular dynamics with NAMD, J. Comput. Chem. 26 (2005) 1781–1802.
[35] N.A. Baker, D. Sept, S. Joseph, M.J. Holst, J.A. McCammon, Electrostatics of nanosystems: application to microtubules and the ribosome, Proc. Natl. Acad. Sci. U. S. A. 98 (2001) 10037–10041.
[36] M. Rostkowski, M.H.M. Olsson, C.R. Sondergaard, J.H. Jensen, Graphical analysis of pH-dependent properties of proteins predicted using PROPKA, BMC Struct. Biol. 11 (2011).
[37] S. Cukierman, Et tu, Grotthuss! and other unfinished stories, Biochim. Biophys. Acta Bioenerg. 1757 (2006) 876–885.
[38] P. Knorzer, A. Silakov, C.E. Foster, F.A. Armstrong, W. Lubitz, T. Happe, Importance of the protein framework for catalytic activity of [FeFe]-hydrogenases, J. Biol. Chem. 287 (2012) 1489–1499.
[39] M.L. Brewer, U.W. Schmitt, G.A. Voth, The formation and dynamics of proton wires in channel environments, Biophys. J. 80 (2001) 1691–1702.
[40] Q. Cui, M. Karplus, Is a "proton wire" concerted or stepwise? A model study of proton transfer in carbonic anhydrase, J. Phys. Chem. B 107 (2003) 1071–1078.
[41] N. Agmon, The Grotthuss mechanism, Chem. Phys. Lett. 244 (1995) 456–462.
[42] J.F. Nagle, H.J. Morowitz, Molecular mechanisms for proton transport in membranes, Proc. Natl. Acad. Sci. U. S. A. 75 (1978) 298–302.
[43] M. Frey, Hydrogenases: hydrogen-activating enzymes, Chembiochem 3 (2002) 153–160.
[44] M. O'Hagan, W.J. Shaw, S. Raugei, S. Chen, J.Y. Yang, U.J. Kilgore, D.L. DuBois, R.M. Bullock, Moving protons with pendant amines: proton mobility in a nickel catalyst for oxidation of hydrogen, J. Am. Chem. Soc. 133 (2011) 14301–14312.
[45] UniProt Consortium, Reorganizing the protein space at the Universal Protein Resource (UniProt), Nucleic Acids Res. 40 (2012) D71–D75.